ACS APPLIED MATERIALS & INTERFACES

Research Article

www.acsami.org

Self-Supported Fibrous Porous Aromatic Membranes for Efficient CO_2/N_2 Separations

Lingbo Meng,[†,‡] Xiaoqin Zou,*[,‡] Shukun Guo,[†] Heping Ma,[§] Yongnan Zhao,[†] and Guangshan Zhu*[,‡]

[†]Institute of Nanostructured Materials & Tianjin Key Laboratory of Fiber Modification and Functional Fiber, School of Materials Science and Engineering, Tianjin Polytechnic University, Tianjin 300387, P. R. China

[‡]Faculty of Chemistry, Northeast Normal University, Changchun 130024, P. R. China

[§]State Key Laboratory of Luminescence and Applications, Changchun Institute of Optics, Fine Mechanics and Physics, Chinese Academy of Sciences, Changchun 130033, P. R. China

Supporting Information

ABSTRACT: In this paper, we describe a new synthesis protocol for the preparation of self-supported hollow fiber membranes composed of porous aromatic framework PAF-56P and PSF. PAF-56P was facilely prepared by the cross-coupling reaction of triangle-shaped cyanuric chloride and linear *p*-terophenyl monomers. The prepared PAF-56P material possesses an extended conjugated network, the structure of which is confirmed by nuclear magnetic resonance and infrared characterizations, as well as a permanent porosity with a BET surface area of 553.4 $m^2 g^{-1}$ and a pore size of 1.2 nm. PAF-56P was subsequently integrated with PSF matrix into PAF-56P/PSF asymmetric hollow fiber membranes via the dry jet-wet quench method employing PAF-56P/PSF suspensions. Scanning electron microscopy studies show that PAF-56P particles are embedded in the PSF matrix to form continuous membranes. Fabricated PAF-56P/PSF membranes were further exploited for CO_2 capture, which was exemplified by gas separations of CO_2/N_2 mixtures. The PAF-56P/PSF membranes show a high selectivity of CO_2 over N_2 with a separation factor of 38.9 due to the abundant nitrogen groups in the PAF-56P framework. A preferred permeance for CO_2 in the binary CO_2/N_2 gas mixture is obtained in the range of 93−141 GPU due to the large CO_2 adsorption capacity and a large pore size of PAF-56P. Additionally, PAF-56P/PSF membranes exhibit excellent thermal and mechanical stabilities, which were examined by thermal analysis and gas separation tests with the dependencies of temperatures and pressures. The merits of high selectivity for CO_2, good stability, and easy scale up make PAF-56P/PSF hollow fiber membranes of great interest for the industrial separations of CO_2 from the gas exhausts.

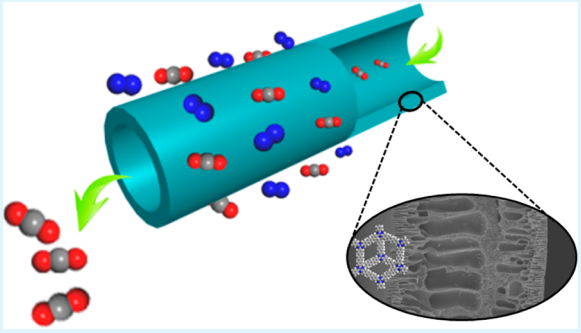

KEYWORDS: *fiber membranes, porous aromatic frameworks, gas separations, CO_2 selectivity, permeance*

1. INTRODUCTION

Porous organic framework materials (POFs) such as covalent organic frameworks (COFs),[1] polymers of intrinsic microporosity (PIMs),[2] conjugated porous polymers (CPPs),[3] porous aromatic frameworks (PAFs),[4] and elemental organic frameworks (EOFs)[5] make up a new class of porous solids, which have recently attracted growing and interdisciplinary interest in different areas, such as adsorption/storage,[6−13] separations,[14−16] chemical sensors,[17] optical devices,[18] and catalysis,[19] because of their large surface areas, low framework densities, and structural diversity as well as high flexibility for incorporating various functional groups at a molecular level.[20,21] PAFs as another subclass of POFs are composed of different aromatic moieties linked by covalent C−C (C−N) bonds, which resulted in rigid skeletons, high thermal and chemical stability, tunable porous structures, etc.[22] The features of permanent porosity and intrinsic polymer characteristics of processing flexibility make this class of porous materials particularly appealing in membrane applications. Thus, the preparation of POFs or PAFs membranes has been proposed via numerous synthetic routes,[23,24] and such materials have been applied in a wide range of research fields, particularly as separating membranes in gas separations.[25−29]

The separation or capture of CO_2 from the flue gas or natural gas is of great interest from the perspective of energy and the environment.[30] Currently, CO_2 separation is a crucial step in fossil fuel conversion via precombustion or postcombustion procedures, which was usually accomplished by a cryogenic method or a sorption approach using different adsorbents.[31,32] Membrane technology is a promising and attractive alternative to the conventional processes mentioned above because of advantages such as greater energy efficiency, a small footprint,

Received: May 13, 2015
Accepted: June 29, 2015
Published: June 29, 2015

DOI: 10.1021/acsami.5b04148
ACS Appl. Mater. Interfaces 2015, 7, 15561−15569

Scheme 1. (a) Representation of the Synthesis Protocol for Preparing PAF-56P and (b) a Molecular Model of a Fragment of a PAF-56P Stacked Structure Showing Its Porous Network (drawn by Materials Studio)

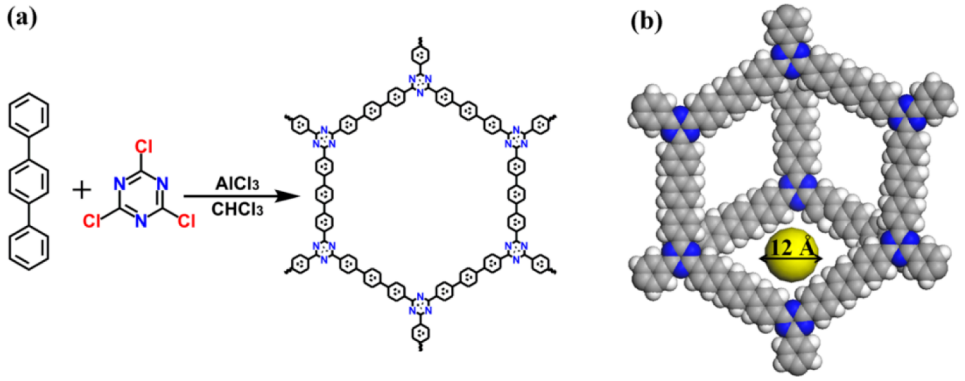

simplicity in operation, ease of scale up, environmental friendliness, and excellent reliability.[33] The separation of CO_2 with a minimized energy expenditure is highly desirable, and therefore, many membranes (such as zeolites,[34] metal organic frameworks,[35] and polymeric membranes[36,37]) have been developed for removing CO_2 from exhaust gas streams. As a special polymer, researchers have attempted to synthesize POF membranes and exploit them in the separation of CO_2 and other light gases because of their high porosity and the ease of processing and cost competitiveness.[38] A promising strategy is to synthesize multicomponent mixed matrix membranes (MMMs) in which a gas-selective porous solid of POFs is embedded in a polymer host.[39,40] Moreover, the active POF phase in the mixed matrix membrane can introduce chemical functionality into the dense polymer to enhance CO_2 permeability and selectivity compared to those of neat polymers in separating and recovering CO_2 from exhaust gases.[41−43]

From an industrial perspective in gas separation, hollow fiber membranes rather than flat sheets are preferred,[44] because they possess higher surface-to-volume ratios, self-mechanical support, and good processability that allows their integration into large-scale compact modules. In the self-supported hollow fiber configuration, no solid support is required for membrane formation, which is in contrast to the supported ones using extra substrates to offer mechanical strength for the entire membrane.[45]

On the basis of the considerations described above, our objective in this study is to synthesize a functional PAF mixed matrix membrane for selective CO_2 capture or separation. In our proposed mixed matrix membrane, an active phase of PAF-56P is selected as a potential candidate for membrane fabrication to achieve the goal of enhanced CO_2 selectivity and improved permeability. PAF-56P constructed from industrial chemicals cyanuric chloride and *p*-terophenyl (the chemical structure of a fragment of PAF-56P is shown in Scheme 1) is a nitrogen-containing polymer that provides active sites for CO_2 sorption. PAF-56P exhibits a three-dimensional framework with a large pore size of 12.0 Å. In addition to the aforementioned scientific issue, polysulfone (PSF Udel P-3500) is chosen as the appropriate continuous phase to overcome some technical hurdles for the preparation of defect-free mixed matrix membranes. The unique properties of its glassy and organic nature, high thermal and chemical stability, and commercial availability render PSF applicable in membrane fabrication because of its processing flexibility and cost competitiveness. Further, PAF-56P/PSF membranes will be prepared in the configuration of asymmetric hollow fibers by combining advantages of both PAF-56P and PSF.[46] CO_2 separation, herein, will be exemplified by PAF-56P/PSF self-supported asymmetric hollow fiber membranes with varied PAF-56P contents under different conditions.

2. EXPERIMENTAL SECTION

2.1. Materials. Glassy polysulfone (PSF) Udel P-3500 was purchased from Acros and dried at 393 K overnight to remove water residues before each use. Anhydrous *N*-methyl-2-pyrrolidinone (NMP), chloroform ($CHCl_3$), dichloromethane (CH_2Cl_2), hexane, methanol (CH_3OH), and ethanol (C_2H_5OH) were obtained from Sigma-Aldrich (Milwaukee, WI) and used without further purification. Polydimethylsiloxane (PDMS, Sylgard184) was received from Dow Corning. *p*-Terophenyl (99%), cyanuric chloride (99%), and aluminum chloride ($AlCl_3$) were purchased from Aladdin, Energy Chemicals, and Tianjin Guangfu Chemicals, respectively.

2.2. Synthesis of PAF-56P. Cyanuric chloride (1.1 g, 6 mmol) and *p*-terophenyl (2.07 g, 9 mmol) were dissolved in 30 mL of $CHCl_3$, and then $AlCl_3$ (2.6 g, 19.5 mmol) was added to the solution described above while it was being constantly stirred and further refluxed for 5 h. The reaction mixture was then cooled to room temperature. The product was filtered by being washed with a NaOH solution (0.1 M), hydrochloric acid (0.1 M), water, ethanol, acetone, and dichloromethane to remove any impurities. Further purification of the product was conducted by Soxhlet extraction using methanol for 12 h. Finally, the product was dried at 353 K overnight to give a brown powder (90% yield). The bulk powder was subsequently crushed into small particles in a ball milling jar for 1 h (QM-3B ball mill apparatus, Nanjing NanDa Instrument Plant).

2.3. Synthesis of PAF-56P/PSF Membranes. Prior to the preparation of PAF-56P/PSF membranes, PAF-56P (small particle powder) was evacuated at room temperature to remove any residual solvent. PSF beads were dried at 393 K overnight to remove adsorbed substances before each use. The detailed protocol for preparing PAF-56P/PSF membranes was as follows: 0.3−2.4 g of PAF-56P was first dispersed in 118.4 g of *N*-methyl-2-pyrrolidinone while being vigorously stirred for 24 h and then treated under ultrasonic conditions for 1 h. Subsequently, 15 g of PSF was added to the mixture described above while being continuously stirred at 333 K until complete dissolution was achieved. The remaining PSF (15 g) was added to the mixture until a uniform suspension was obtained. After the temperature was decreased to 303 K, an additional 9.5 g of ethanol was introduced into the suspension while it was being further stirred at 303 K for 1 day to homogenize the suspension. The loading amount of PAF-56P was in the range of 1−8 wt % of the whole PSF and denoted as 1−8 wt % PAF-56P@PSF, respectively. A pure PSF membrane was prepared in the same manner using a PSF solution composed of 19 wt % polysulfone, 75 wt % *N*-methyl-2-pyrrolidinone

DOI: 10.1021/acsami.5b04148
ACS Appl. Mater. Interfaces 2015, 7, 15561−15569

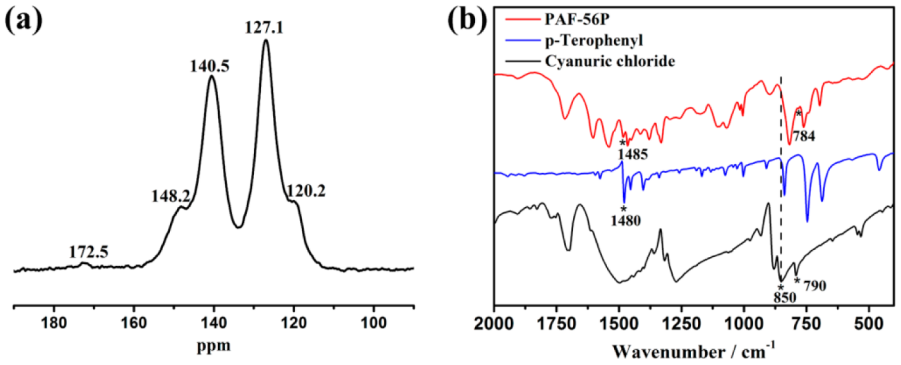

Figure 1. (a) ^{13}C solid-state MAS NMR spectrum of as-synthesized PAF-56P. (b) FT-IR spectra of cyanuric chloride, *p*-terophenyl reactants, and the PAF-56P product.

(NMP), and 6 wt % ethanol. The compositions of the spinning solution are listed in Table S1 of the Supporting Information.

PAF-56P/PSF or PSF solutions were spun to produce self-supported asymmetric hollow fiber membranes via the dry jet-wet quench method.[47] Prepared solutions or suspensions (PAF-56P/PSF or PSF) were extruded into constant and continuous flows via a syringe pump. The spinning temperature (i.e., 298 K) was measured by a thermocouple. The solution flows extruded by spinneret first passed through a preadjustment air gap and then went into a coagulation bath under a guide roller. Additional core liquid was introduced into the inner side of extruded solution flows to generate hollow fibers. The nascent fibers were collected after water quenching (coagulation bath) by the rotating drum. A detailed scheme of the spinning apparatus is provided in the Figure S1 of the Supporting Information. The spinning parameters are summarized in Table S2 of the Supporting Information. The fibers removed from the drum by cutting cleanly using a sharp blade were subjected to a further post-treatment. The residual NMP solvent occluded in the fibers was successively exchanged with water, methanol, and hexane. The typical procedure includes first immersing the fibers in deionized water for 3 days (water was changed every day) and then immersing for 30 min each in three successive aliquots (400 mL) of methanol, followed by 30 min each in three aliquots (400 mL) of hexane. The fibers were removed from the last hexane bath and allowed to dry at ambient temperature overnight. To seal any large pinhole defects in the selective surface layer, the dried hollow fibers (40 cm in length) of PAF-56P/PSF membranes as well as the PSF reference were immersed in a coating solution that contains 3 wt % polydimethylsiloxane (PDMS) in hexane.[48]

2.4. Characterizations. Solid-state ^{13}C CP/MAS nuclear magnetic resonance (NMR) measurements were conducted on a Bruker Avance III model 400 MHz NMR spectrometer at a MAS rate of 5 kHz. The Fourier transform infrared (FT-IR) spectra were collected on a Bruker IFS 66 V/S Fourier transform infrared spectrometer with KBr pellets in the range of 4000−400 cm^{-1}. The gas sorption isotherms were measured on a Quantachrome Autosorb iQ2 analyzer. Prior to the measurements, the samples were degassed at 393 K for 24 h. N_2 sorption isotherms were recorded at 77, 273, and 298 K; CO_2 sorption measurements were performed at 273 and 298 K. Ultra-high-purity grade (99.99%) N_2 and CO_2 gases were used for all adsorption measurements. A liquid nitrogen bath was utilized to control the temperature at 77 K. Ice−water and water baths equipped with a temperature sensor were used to control the temperature at 273 and 298 K. The surface area, micropore volume, and pore size of PAF-56P were calculated from N_2 adsorption isotherms (77 K) using BET, t-plot, and NL-DFT methods, respectively. Scanning electron microscopy (SEM) imaging was performed on a JEOL JSM 6700 instrument. Elemental analyses (C, H, N) of PSF, PAF-56P, and PAF-56P/PSF bulk samples were conducted on a PerkinElmer 240 analyzer. Thermogravimetric analysis was implemented using a Netzch Sta 449c thermal analyzer system at a heating rate of 10 K min^{-1} under air.

2.5. Gas Separations. Prior to gas separations, membranes were dehydrated in a vacuum oven at 393 K and 10^{-5} Pa overnight to remove adsorbed water. And then, PAF-56P/PSF or PSF membranes were fixed in a membrane chamber and sealed with xylene resistant fluorocarbon O-rings and connected to a gas flow system (a setup scheme was detailed in Figure S2 of the Supporting Information). Single or binary gas mixtures of CO_2 and N_2 were introduced into the membrane module in the feed side, and the permeate was carried by argon sweep gas. The feed and permeate gases were analyzed by online gas chromatography (GC-450, BRUKER). The feed pressures were monitored by a pressure gauge, and the temperature of the membrane chamber was measured by a thermocouple. The values of separation factors (CO_2/N_2) and gas permeances (CO_2 or N_2) reported here are the average numbers of three consecutive measurements.

3. RESULTS AND DISCUSSION

3.1. General Characterizations of PAF-56P. Triangle and linear building blocks are employed to build porous aromatic frameworks via cross-coupling reaction. Additionally, the functional groups in the building blocks and their connection modes determine the physicochemical properties of aromatic frameworks. On the basis of this consideration, PAF-56P was prepared by the reaction of cyanuric chloride as the triangle node and *p*-terophenyl as the linear linker via Sonogashira−Hagihara cross coupling (Scheme 1).[49] For better illustration of the connectivity and geometry of carbon atoms in the PAF-56P structure, this PAF material was characterized by solid-state ^{13}C cross-polarization magic-angle spinning (CP/MAS) NMR and Fourier transform infrared spectroscopies. Figure 1a shows the ^{13}C CP/MAS NMR spectrum of the PAF-56P solid sample. The chemical shift at 172.5 ppm is observed in the NMR spectrum, which is assigned to the carbon atom in cyanuric groups; other chemical shifts associated with carbon atoms in benzene rings are detected at 120.2, 127.1, 140.5, and 148.2 ppm. This observation indicates that the main components of the PAF-56P backbone are cyanuric and *p*-terophenyl moieties after the reaction. The PAF-56P solid is further investigated by FT-IR spectroscopy. The infrared (IR) spectra of as-prepared PAF-56P and their starting monomers are shown in Figure 1b. The band centered at 850 cm^{-1} associated with C−Cl vanishes into the background of the PAF-56P product by taking cyanuric chloride as a reference.

IR bands attributed to the C−C (1485 cm^{-1}) stretching vibration in the benzene ring and cyanuric ring deformation (784 cm^{-1}) in the as-synthesized PAF-56P product are similar to those in *p*-terophenyl and cyanuric chloride monomers, which suggests that N-containing groups are kept intact, offering adsorption sites for CO_2. Combining results of NMR

DOI: 10.1021/acsami.5b04148
ACS Appl. Mater. Interfaces 2015, 7, 15561−15569

and IR studies, we can conclude that the reaction between cyanuric chloride and *p*-terophenyl precursors is completed, indicated by the total disappearance of C−Cl signals, and thus an extended conjugated framework (PAF-56P) is formed.

The porosity and pore structures of PAF-56P were investigated by the nitrogen sorption measurement at 77 K. As shown in Figure 2, PAF-56P exhibits type I isotherms with a

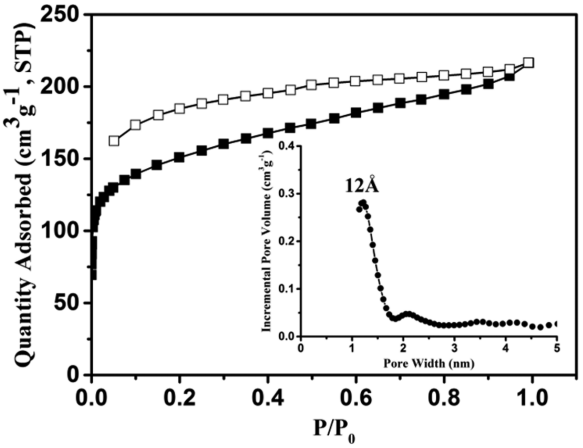

Figure 2. N_2 adsorption isotherms of PAF-56P at 77 K and the pore size distribution calculated by the NL-DFT method (see the inset).

sharp uptake at low relative pressures followed by a steady adsorption at high pressures, which is the typical feature of microporous materials.

For clear illustration, a series of pore parameters derived from the nitrogen isotherms are listed in Table S3 of the Supporting Information, including Langmuir and Brunauer−Emmett−Teller (BET) surface areas, pore sizes, total pore volumes, and micropore volumes. The Langmuir and BET surface areas of PAF-56P are calculated to be 624.5 and 553.4 $m^2\ g^{-1}$, respectively. The pore diameter is estimated to be around 1.2 nm as shown by the dominant peak in the size distribution curve (the inset in Figure 2), and the total pore volume is 0.3 $cm^3\ g^{-1}$. The results of N_2 adsorption provide direct evidence that PAF-56P is a highly porous material.

The morphology and the size of as-synthesized PAF-56P particles are visualized by SEM. Spherelike nanoparticles are prepared after ball milling, and the size of an individual one is around 100−400 nm (Figure 3a), which guarantees facile fabrications of homogeneous membranes using a stable suspension (see the inset in Figure 3a). PAF-56P/PSF self-supported hollow fiber membranes are prepared by extruding a PAF-56P/PSF solution with varied contents from 0 to 8 wt % into constant and continuous flows (Table S1 of the Supporting Information), followed by a further quenching process in a coagulation bath. The optical picture (Figure 3b) shows that the length and outer diameter of tested PAF-56P/PSF fiber membrane are 40 cm and 1 mm, respectively, and both values can be easily adjusted by changing the injecting parameters (Table S2 of the Supporting Information). The insight structures of the fiber membrane are inspected by SEM in detail.

Figure 3c shows a top view of the outer surface of a representative membrane with 5 wt % PAF-56P. PAF-56P particles are embedded in a PSF matrix (marked by circles). No visible cracks or tears are observed, indicative of a homogeneous PAF-56P/PSF membrane, which makes this membrane appropriate for the subsequent gas separation. Panels d and e of Figure 3show side views of the same PAF-56P/PSF fiber membrane at low and high magnifications, respectively. The fiber membrane exhibits a nest morphology, composed of inner, supporting (fingerlike areas of sections 1 and 2 in Figure 3d) and outer (also called selective skin) layers. The thickness of the entire membrane is ∼128 μm, and the effective thickness of the selective skin layer is ∼1.0 μm. Looking closely, one can see that PAF-56P particles are merged with the PSF matrix to form a continuous layer (inset in Figure 3e), indicating that PAF-56P and PSF are compatible and there is good adhesion between the two polymers. Dense PAF-56P particles are encapsulated in overlapped multilayers of the supporting layer, as shown in the fingerlike regions of sections 1 and 2 (Figure 3f). Other membranes with different PAF-56P contents were prepared in the same manner, and their surface features were also determined by SEM (Figure S3 of the Supporting Information). Chemical compositions and thermal stabilities of a series of PAF-56P/PSF membranes were identified by elemental (Table S4 of the Supporting Information) and thermogravimetric (TG) analyses (Figure S4 of the Supporting Information), respectively. With more PAF-56P occluded in the membrane, more nitrogen-containing groups are available, which is in agreement with the increasing ratios of N to C (Table S4 of the Supporting Information). No visible weight loss is observed in the TG curves of PAF-56P/PSF membranes before 773 K, indicating that all prepared membranes can be stable up to 773 K. The better thermal stability of PAF-56P/PSF membranes in comparison to that of neat PAF-56P can be attributed to the contribution of the robust PSF matrix.

To explore the potentiality of PAF-56P/PSF membranes in CO_2 separations, the molecular recognition of PAF-56P toward CO_2 was probed by gas adsorption measurements.

Figure 4a presents adsorption−desorption isotherms of CO_2 and N_2 at 298 K. From the isotherms, it can be found that PAF-56P exhibits high sorption capacity for CO_2 with an uptake of 33 $cm^3\ g^{-1}$ at a P/P_0 of 1.0, which benefits from the abundant basic N sites in the framework. N_2 sorption measurements were conducted in the same way, and the result is depicted in Figure 4a. In contrast to the high rate of uptake for CO_2, PAF-56P exhibits low adsorption affinity for N_2, which is evidenced by a small sorption amount of 2 $cm^3\ g^{-1}$ (P/P_0 = 1.0). The poor adsorption ability of PAF-56P toward N_2 is reasonable, because N_2 (17.6×10^{-25} cm^3) has a polarizability smaller than that of CO_2 (26.3×10^{-25} cm^3); thus, weaker interaction between PAF-56P and N_2 molecules would be expected. Adsorption selectivity is another important index for the evaluation of sorption affinity for one sorbate versus another in ideal gas mixtures. Adsorption selectivity of CO_2 over N_2 in our study is calculated from single-component adsorption isotherms using ideal adsorption solution theory (IAST), which is well recognized and employed to predict gas mixture adsorption behaviors in porous materials.[50] Figure 4b demonstrates the evolution of adsorption selectivities as a function of bulk pressures for the binary CO_2/N_2 gas mixture with an equimolar ratio. PAF-56P shows a very high selectivity of 46 for CO_2 over N_2 at 101 kPa. The high adsorption selectivity toward CO_2 can be attributed to the presence of basic nitrogen sites in the PAF-56P framework, which can create a strong and directed interaction between CO_2 molecules and nitrogen atoms. Meanwhile, the stronger van der Waals force favors more

DOI: 10.1021/acsami.5b04148
ACS Appl. Mater. Interfaces 2015, 7, 15561−15569

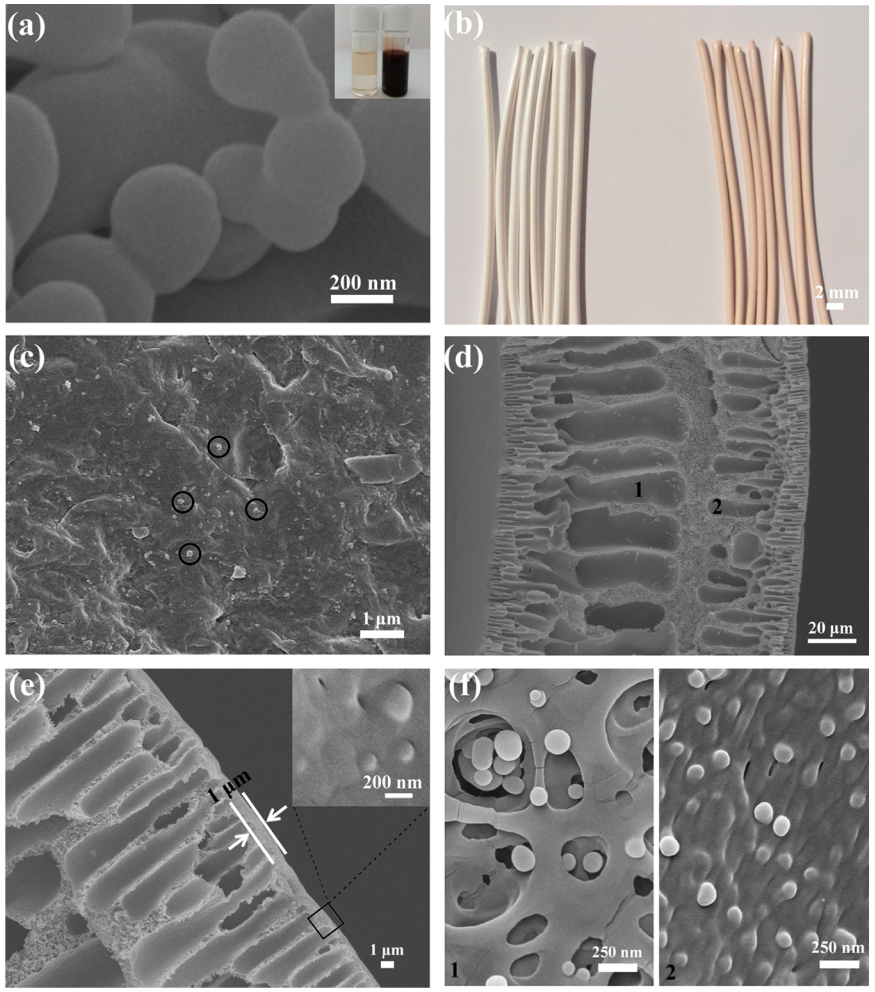

Figure 3. (a) SEM image of an as-synthesized PAF-56P solid sample and its suspension in *N*-methyl-2-pyrrolidinone [inset picture of PSF (left) and PAF-56P/PSF (5 wt %, right) solutions]. (b) Optical photos of pure PSF (left) and PAF-56P/PSF fiber membranes (right). (c) Top SEM view of the outer surface (some representative PAF-56P particles are shown in circles). (d and e) Side views of the PAF-56P/PSF membrane with 5 wt % PAF-56P. (f) Enlarged images of the cross-sectional areas of sections 1 and 2 in panel d.

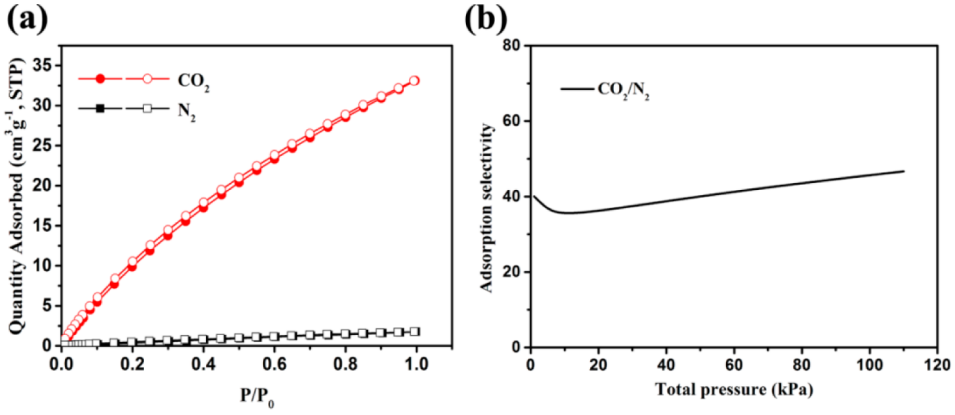

Figure 4. (a) Adsorption−desorption isotherms of CO_2 and N_2 on PAF-56P at 298 K (filled and empty symbols represent adsorption and desorption branches, respectively). (b) Sorption selectivity of CO_2 over N_2 on PAF-56P predicted by IAST calculation.

closely packed CO_2 molecules in the pores of PAF-56P, which resulted in a higher sorption capacity of CO_2 over N_2.[51]

3.2. Gas Separations. Encouraged by the results obtained from gas adsorption measurements and IAST prediction, we prepared PAF-56P/PSF membranes and conducted gas permeation tests, which were exemplified by single gases (CO_2 or N_2) and their gas mixture. The permeation results for gases CO_2 and N_2 through the PAF-56P/PSF membrane with 5 wt % PAF-56P are summarized in Table 1.

As shown in Table 1, the single-gas permeance of CO_2 is quite close to that of its gas mixture, while the permeance of N_2 is lowered significantly from that of CO_2 [12.3 vs 156.9 GPU, 1

DOI: 10.1021/acsami.5b04148
ACS Appl. Mater. Interfaces 2015, 7, 15561−15569

Table 1. Gas Permeances and Separation Factors in Single Gases and a Gas Mixture for the Representative PAF-56P/PSF Membrane with 5 wt % PAF-56P at Room Temperature (293 K), a Pressure Drop of 0.06 MPa, and a Gas Volume Ratio of 1:1

	CO_2	N_2
mixture gas permeance (GPU)	132.2 ± 4.3	3.4 ± 0.2
single-gas permeance (GPU)	156.9 ± 0.5	12.3 ± 0.5
separation factor	38.9 ± 3.1	
ideal separation factor	12.7 ± 0.6	
Knudsen constant	1.25	

GPU = 1×10^{-6} cm^3 (STP) cm^{-2} s^{-1} $cmHg^{-1}$], indicating that the PAF-56P/PSF membrane exhibits permeation priority toward CO_2, which is in accordance with the better adsorption capacity for CO_2 in PAF-56P (Figure 4a). The ideal separation factor of 12.7 for CO_2 over N_2 on the PAF-56P/PSF membrane is higher than that of the neat PSF membrane (a measured value of 6.0), suggesting a large contribution of PAF-56P introduced in the mixed matrix membrane. Further, both separation factors (12.7 and 38.9) of the PAF-56P/PSF membrane greatly exceed the Knudsen constant (1.25), suggesting that the as-prepared PAF-56P/PSF membrane displays good quality (continuous and compact) and is suitable for gas separations. The gas separation factor of its binary mixture is calculated to be 38.9 (Table 1); surprisingly, this value is ~2 times higher than that of CO_2 and N_2 single gases (12.7). This finding can be rationalized as the preferential selective sorption of CO_2 in PAF-56P being enhanced by a strong interaction with cyanuric groups;[52] namely, CO_2 molecules are preferentially adsorbed and permeate through the membrane, thereby hindering N_2 transport in a mixed gas environment via a competitive adsorption mode. Meanwhile, the separation factor of the gas mixture (38.9) is very close to the adsorption selectivity of ideal gas mixture (46) predicted by IAST calculation, which suggests that CO_2 selectivity of the PAF-56P/PSF membrane is mainly governed by CO_2 adsorption. It is noteworthy that the PAF-56P/PSF membrane demonstrates a high permeance of CO_2 among the state-of-the-art mixed matrix membranes for the separations of CO_2/N_2 mixtures (Table S5 of the Supporting Information). The high CO_2 permeance can be attributed to the large pore size of 1.2 nm in PAF-56P.

3.3. Effect of Content on CO_2 Separation. The same preparation protocol was employed for the fabrication of PAF-56P/PSF membranes with varied PAF-56P contents. Figure 5 presents the separation results of different membranes with PAF-56P contents that varied from 0 to 8 wt %. CO_2 permeance shows an increasing trend (from 61.6 to 140.5 GPU) with more PAF-56P particles introduced into the membranes, indicating that PAF-56P facilitates the permeation of CO_2 because of the high porosity and specific sorption affinity.

The separation factors are increasing gradually from 10.6 to 38.9 with increasing PAF-56P contents and reach maxima at a content of 5 wt %. The expected higher separation factors are due to more selective permeation of CO_2 through the membranes when denser basic nitrogen groups are present in PAF-56P/PSF membranes. A lower separation factor of 2.3 is also observed for the membrane with a PAF-56P content of 8 wt %. The weakened separating ability probably exists because of an occurrence of some cracks between PAF-56P particles

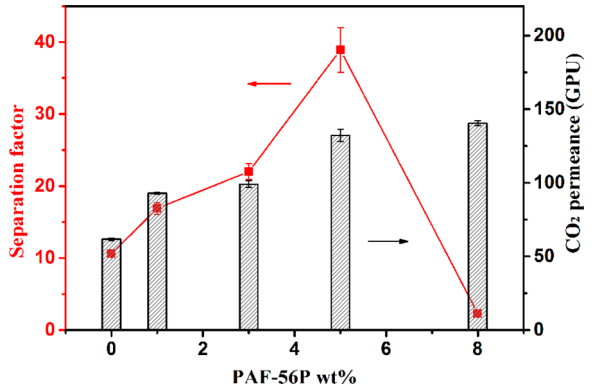

Figure 5. Separation performances of PAF-56P/PSF membranes with different PAF-56 contents at 293 K for CO_2/N_2 gas mixtures (gas volume ratio of 1:1).

and the PSF matrix induced by the aggregation of PAF particles (Figure S3d of the Supporting Information). This possible reason for the low separation factor is further supported by a rapid drop in Young's modulus (Figure S5 of the Supporting Information) when the PAF-56P content is approaching 8 wt %.[38]

3.4. Effect of Pressure on CO_2 Separation. To evaluate the mechanical stability of self-supported PAF-56P/PSF fiber membranes, CO_2 separation tests of pressure dependence were conducted by increasing the feed pressure from 0.06 to 0.16 MPa. As shown in Figure 6, it is found that the permeance for CO_2 slightly increases from 132.2 to 152.5 GPU.

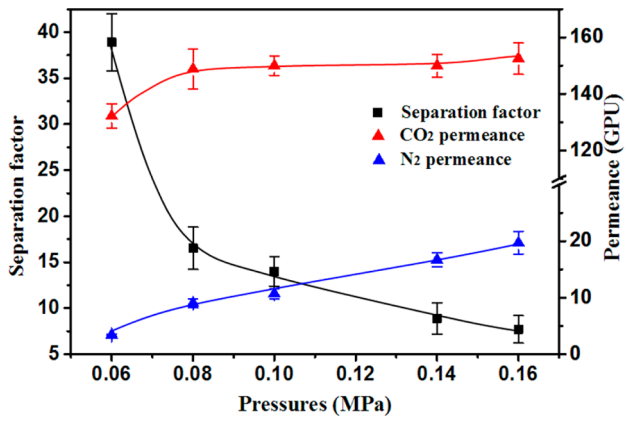

Figure 6. Gas permeances and separation factors of a representative PAF-56P/PSF membrane (5 wt % PAF-56P) for CO_2/N_2 gas mixtures at different pressures (gas volume ratio of 1:1).

Correspondingly, the permeance of N_2 also increases, but at a higher magnitude (from 3.4 to 19.7 GPU), leading to a decrease in the CO_2/N_2 separation factor. The behavior for a lower separation factor of CO_2 versus N_2 at a higher pressure can be interpreted with the fact that the sorption capacity of a PAF-56P/PSF membrane for N_2 increases more than that for CO_2 with an increase in pressure, which resulted in enhanced N_2 permeance in the PSF matrix via a gas solution−diffusion approach.[53] It is worth mentioning that the membrane regains the separation factor of CO_2/N_2 and CO_2 permeance upon releasing the pressure to 0.06 MPa [Figure S6a (2) of the Supporting Information], which shows us that the self-supported PAF-56P/PSF fiber membrane is stable under pressure.

DOI: 10.1021/acsami.5b04148
ACS Appl. Mater. Interfaces 2015, 7, 15561−15569

3.5. Thermal Effect on CO_2 Separation. To address the thermal behaviors of PAF-56P/PSF membranes, we evaluated the permeations at different temperatures (from 293 to 353 K). Figure 7 depicts the dependence of gas permeances and separation factors on test temperatures in the gas mixture of CO_2 and N_2 using a PAF-56P/PSF membrane with 5 wt % PAF-56 at a constant pressure of 0.06 MPa. It is found that the permeance for CO_2 remains quite constant (132.2−150.8 GPU) over the whole temperature range, suggesting that CO_2 permeation is largely influenced by the surface adsorption of CO_2 rather than its diffusion.

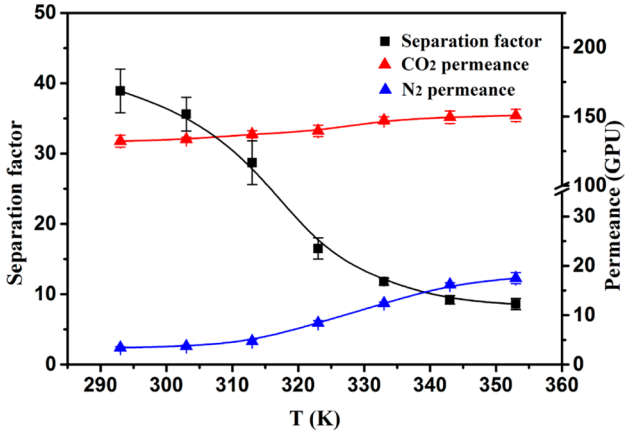

Figure 7. Gas permeances and separation factors of the PAF-56P/PSF membrane (5 wt %) for CO_2/N_2 gas mixtures at different temperatures (gas volume ratio of 1:1, pressure drop of 0.06 MPa).

In contrast, the permeance for N_2 increases markedly (3.4−17.5 GPU) from 293 to 353 K (Figure 7), which can be explained by the dominant effect of an increased diffusion rate (gas fugacity) within large pores (1.2 nm) during the gas permeation process.[54] The inverse effect of increased N_2 permeance to constant CO_2 permeance leads to a decrease in the separation factor of CO_2 over N_2 as the temperature is elevated from 293 to 353 K. In addition, the fiber membrane was not damaged by the high-temperature testing, evidenced by the preserved performance after returning to the low temperature of 293 K [Figure S6b (2) of the Supporting Information].

3.6. Reproducibility and Robustness of the PAF-56/PSF Membrane. To examine the reproducibility and robustness of self-supported PAF-56/PSF fiber membranes, we conducted the binary gas mixture permeations on the PAF-56/PSF membrane with 5 wt % PAF-56P via continuous testing with time.

The permeation data for the CO_2/N_2 mixture at room temperature (293 K) with a pressure drop of 0.06 MPa are presented in Figure 8. As shown, the PAF-56P/PSF membrane retains the separation factor (~38) and CO_2 permeance at a high value (~126 GPU) over a period of 8 days. The long durability of the membrane with repetitive uses proves that the self-supported PAF-56/PSF fiber membranes possess high mechanical stability, making this type of PAF membrane promising for CO_2 separation or capture in industrial applications.

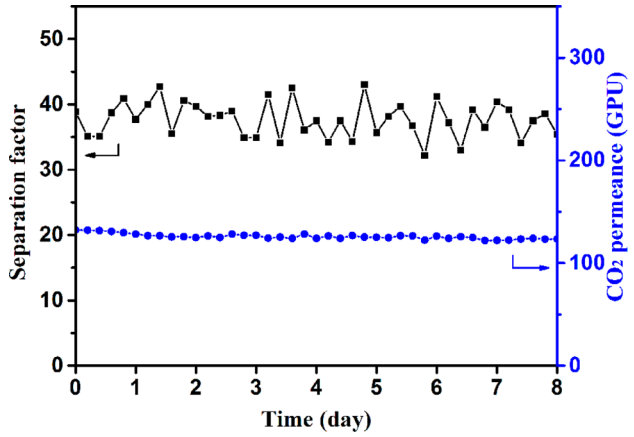

Figure 8. Gas permeances and separation factors of the PAF-56P/PSF membrane (5 wt %) for CO_2/N_2 gas mixtures as a function of test time (gas volume ratio of 1:1, pressure drop of 0.06 MPa).

4. CONCLUSIONS

In conclusion, we have demonstrated the feasibility of fabricating self-supported porous aromatic framework membranes. The preparation of a PAF-56P/PSF POF membrane has been exemplified by introducing PAF-56P particles with permanent micropores into a PSF matrix via the dry jet-wet quench method. A conjugated backbone of PAF-56P material has been achieved by cross coupling of cyanuric chloride and *p*-terophenyl monomers. NMR, IR, and elemental analyses have confirmed that PAF-56P possesses accessible nitrogen groups in the framework. Gas sorption measurements and IAST calculation have shown that PAF-56P exhibits high sorption capacity and affinity for CO_2 because of its large surface area and basic nitrogen atoms. Gas separation results have revealed that the PAF-56P/PSF membrane shows a superior separation performance, including a high separation factor (as high as 38.9), and improved CO_2 permeance in the range of 132−151 GPU for CO_2/N_2 gas mixtures at 293−353 K. Favorable CO_2 permeation through the PAF-56P/PSF membrane is a consequence of the preferential adsorption of CO_2 in the micropores and simultaneous inhibition of N_2 permeation from CO_2/N_2 mixtures when the competitive adsorption takes place during a stable separation process. The self-supported PAF-56P/PSF hollow fiber membranes are reproducible and display high thermal and mechanical stabilities, showing its potential in the practical application of CO_2 separation.

■ ASSOCIATED CONTENT

Ⓢ Supporting Information

Setup schemes for membrane preparation and gas separation and discussed data, including SEM images, TG curves, separation results, chemical compositions of membranes, and physicochemical properties of PAF-56P membranes. The Supporting Information is available free of charge on the ACS Publications website at DOI: 10.1021/acsami.5b04148.

■ AUTHOR INFORMATION

Corresponding Authors

*E-mail: xiaoqinzou123@gmail.com.
*E-mail: zhugs100@nenu.edu.cn.

Notes

The authors declare no competing financial interest.

DOI: 10.1021/acsami.5b04148
ACS Appl. Mater. Interfaces 2015, 7, 15561−15569

■ ACKNOWLEDGMENTS

We are grateful for the financial support from the National Basic Research Program of China (973 Program, Grants 2012CB821700 and 2014CB931800) and the Major International (Regional) Joint Research Project of NSFC (Grant 21120102034).

■ REFERENCES

(1) Côté, A. P.; Benin, A. I.; Ockwig, N. W.; O'Keeffe, M.; Matzger, A. J.; Yaghi, O. M. Porous, Crystalline, Covalent Organic Frameworks. *Science* **2005**, *310*, 1166−1170.
(2) Budd, P. M.; Ghanem, B. S.; Makhseed, S.; McKeown, N. B.; Msayib, K. J.; Tattershall, C. E. Polymers of Intrinsic Microporosity (PIMs): Robust, Solution-Processable, Organic Nanoporous Materials. *Chem. Commun.* **2004**, *2*, 230−231.
(3) Cooper, A. I. Conjugated Microporous Polymers. *Adv. Mater.* **2009**, *21*, 1291−1295.
(4) Ben, T.; Ren, H.; Ma, S.; Cao, D.; Lan, J.; Jing, X.; Wang, W.; Xu, J.; Deng, F.; Simmons, J. M.; Qiu, S.; Zhu, G. Targeted Synthesis of A Porous Aromatic Framework with High Stability and Exceptionally High Surface Area. *Angew. Chem., Int. Ed.* **2009**, *48*, 9457−9460.
(5) Wu, D.; Xu, F.; Sun, B.; Fu, R.; He, H.; Matyjaszewski, K. Design and Preparation of Porous Polymers. *Chem. Rev.* **2012**, *112*, 3959−4015.
(6) Bojdys, M. J.; Jeromenok, J.; Thomas, A.; Antonietti, M. Rational Extension of the Family of Layered, Covalent, Triazine-Based Frameworks with Regular Porosity. *Adv. Mater.* **2010**, *22*, 2202−2205.
(7) Dawson, R.; Cooper, A. I.; Adams, D. J. Nanoporous Organic Polymer Networks. *Prog. Polym. Sci.* **2012**, *37*, 530−563.
(8) Xiang, Z. H.; Zhou, X.; Zhou, C. H.; Zhong, S.; He, X.; Qin, C. P.; Cao, D. P. Covalent-Organic Polymers for Carbon Dioxide Capture. *J. Mater. Chem.* **2012**, *22*, 22663−22669.
(9) Wood, C. D.; Tan, B.; Trewin, A.; Niu, H.; Bradshaw, D.; Rosseinsky, M. J.; Khimyak, Y. Z.; Campbell, N. L.; Kirk, R.; Stockel, E.; Cooper, A. I. Hydrogen Storage in Microporous Hypercrosslinked Organic Polymer Networks. *Chem. Mater.* **2007**, *19*, 2034−2048.
(10) Thomas, A. Functional Materials: From Hard to Soft Porous Frameworks. *Angew. Chem., Int. Ed.* **2010**, *49*, 8328−8344.
(11) Luo, Y.; Li, B.; Wang, W.; Wu, K.; Tan, B. Hypercrosslinked Aromatic Heterocyclic Microporous Polymers: A New Class of Highly Selective CO_2 Capturing Materials. *Adv. Mater.* **2012**, *24*, 5703−5707.
(12) Li, L.; Cai, K.; Wang, P.; Ren, H.; Zhu, G. Construction of Sole Benzene Ring Porous Aromatic Frameworks and Their High Adsorption Properties. *ACS Appl. Mater. Interfaces* **2015**, *7*, 201−208.
(13) Saleh, M.; Lee, H. M.; Kemp, K. C.; Kim, K. S. Highly Stable CO_2/N_2 and CO_2/CH_4 Selectivity in Hyper-Cross-Linked Heterocyclic Porous Polymers. *ACS Appl. Mater. Interfaces* **2014**, *6*, 7325−7333.
(14) Li, B.; Zhang, Y.; Krishna, R.; Yao, K.; Han, Y.; Wu, Z.; Ma, D.; Shi, Z.; Pham, T.; Space, B.; Liu, J.; Thallapally, P. K.; Liu, J.; Chrzanowski, M.; Ma, S. Introduction of π-Complexation into Porous Aromatic Framework for Highly Selective Adsorption of Ethylene over Ethane. *J. Am. Chem. Soc.* **2014**, *136*, 8654−8660.
(15) Chen, Q.; Wang, Q.; Luo, M.; Mao, L.; Yan, C.; Li, Z.; Han, B. Microporous Polymeric Microsphere via Surfactant-Free Suzuki Coupling Polymerization in a Single-phase: Porosity and Gas Uptake. *Polymer* **2012**, *53*, 2032−2037.
(16) Zhao, Y. F.; Yao, K.; Teng, B.; Zhang, T.; Han, Y. A Perfluorinated Covalent Triazine-Based Framework for Highly Selective and Water-Tolerant CO_2 Capture. *Energy Environ. Sci.* **2013**, *6*, 3684−3692.
(17) Yuan, Y.; Ren, H.; Sun, F.; Jing, X.; Cai, K.; Zhao, X.; Wang, Y.; Wei, Y.; Zhu, G. Sensitive Detection of Hazardous Explosives via Highly Fluorescent Crystalline Porous Aromatic Frameworks. *J. Mater. Chem.* **2012**, *22*, 24558−24562.
(18) Wan, S.; Gándara, F.; Asano, A.; Furukawa, H.; Saeki, A.; Dey, S. K.; Liao, L.; Ambrogio, M. W.; Botros, Y. Y.; Duan, X.; Seki, S.; Stoddart, J. F.; Yaghi, O. M. Covalent Organic Frameworks with High Charge Carrier Mobility. *Chem. Mater.* **2011**, *23*, 4094−4097.
(19) Kaur, P.; Hupp, J. T.; Nguyen, S. T. Porous Organic Polymers in Catalysis: Opportunities and Challenges. *ACS Catal.* **2011**, *1*, 819−835.
(20) Feng, X.; Ding, X.; Jiang, D. Covalent Organic Frameworks. *Chem. Soc. Rev.* **2012**, *41*, 6010−6022.
(21) Zou, X. Q.; Ren, H.; Zhu, G. Topology-Directed Design of Porous Organic Frameworks and Their Advanced Applications. *Chem. Commun.* **2013**, *49*, 3925−3936.
(22) Ben, T.; Qiu, S. Porous Aromatic Frameworks: Synthesis, Structure and Functions. *CrystEngComm* **2013**, *15*, 17−26.
(23) Hao, D. D.; Zhang, J. N.; Lu, H.; Leng, W. G.; Ge, R. L.; Dai, X. N.; Gao, Y. N. Fabrication of a COF-5 Membrane on a Functionalized α-Al_2O_3 Ceramic Support Using a Microwave Irradiation Method. *Chem. Commun.* **2014**, *50*, 1462−1464.
(24) Guiver, M. D.; Lee, Y. M. Polymer Rigidity Improves Microporous Membranes. *Science* **2013**, *339*, 284−285.
(25) Lindemann, P.; Tsotsalas, M.; Shishatskiy, S.; Abetz, V.; Krolla-Sidenstein, P.; Azucena, C.; Monnereau, L.; Beyer, A.; Gölzhäuser, A.; Mugnaini, V.; Gliemann, H.; Bräse, S.; Wöll, C. Preparation of Freestanding Conjugated Microporous Polymer Nanomembranes for Gas Separation. *Chem. Mater.* **2014**, *26*, 7189−7193.
(26) Hart, K. E.; Colina, C. M. Ionomers of Intrinsic Microporosity: In Silico Development of Ionic-Functionalized Gas-Separation Membranes. *Langmuir* **2014**, *30*, 12039−12048.
(27) Du, N.; Dal-Cin, M. M.; Pinnau, I.; Nicalek, A.; Robertson, G. P.; Guiver, M. D. Azide-based Cross-Linking of Polymers of Intrinsic Microporosity (PIMs) for Condensable Gas Separation. *Macromol. Rapid Commun.* **2011**, *32*, 631−636.
(28) Zhu, X.; Tian, C.; Mahurin, S. M.; Chai, S.; Wang, C.; Brown, S.; Veith, G. M.; Luo, H.; Dai, S. A Superacid-Catalyzed Synthesis of Porous Membranes Based on Triazine Frameworks for CO_2 Separation. *J. Am. Chem. Soc.* **2012**, *134*, 10478−10484.
(29) Carta, M.; Malpass-Evans, R.; Croad, M.; Rogan, Y.; Jansen, J. C.; Bernardo, P.; Bazzarelli, F.; McKeown, N. B. An Efficient Polymer Molecular Sieve for Membrane Gas Separations. *Science* **2013**, *339*, 303−307.
(30) Bae, Y.; Snurr, R. Q. Development and Evaluation of Porous Materials for Carbon Dioxide Separation and Capture. *Angew. Chem., Int. Ed.* **2011**, *50*, 11586−11596.
(31) White, D. C. M.; Strazisar, B. R.; Granite, E. J.; Hoffman, J. S.; Pennline, H. W. Separation and Capture of CO_2 from Large Stationary Sources and Sequestration in Geological Formations-Coalbeds and Deep Saline Aquifers. *J. Air Waste Manage. Assoc.* **2003**, *53*, 645−715.
(32) Liang, Z. J.; Marshall, M.; Chaffee, A. L. CO_2 Adsorption-Based Separation by Metal Organic Framework (Cu-BTC) versus Zeolite (13X). *Energy Fuels* **2009**, *23*, 2785−2789.
(33) Baker, R. W. Future Directions of Membrane Gas Separation Technology. *Ind. Eng. Chem. Res.* **2002**, *41*, 1393−1411.
(34) Li, Y.; Yang, W. Microwave Synthesis of Zeolite Membranes: A Review. *J. Membr. Sci.* **2008**, *316*, 3−17.
(35) Al-Maythalony, B. A.; Shekhah, O.; Swaidan, R.; Belmabkhout, Y.; Pinnau, I.; Eddaoudi, M. Quest for Anionic MOF Membranes: Continuous sod-ZMOF Membrane with CO_2 Adsorption-Driven Selectivity. *J. Am. Chem. Soc.* **2015**, *137*, 1754−1757.
(36) Powell, C. E.; Qiao, G. G. Polymeric CO_2/N_2 Gas Separation Membranes for The Capture of Carbon Dioxide from Power Plant Flue Gases. *J. Membr. Sci.* **2006**, *279*, 1−49.
(37) Du, N. Y.; Park, H. B.; Dal-Cin, M. M.; Guiver, M. D. Advances in High Permeability Polymeric Membrane Materials for CO_2 Separations. *Energy Environ. Sci.* **2012**, *5*, 7306−7322.
(38) Gao, X.; Zou, X.; Ma, H.; Meng, S.; Zhu, G. Highly Selective and Permeable Porous Organic Framework Membrane for CO_2 Capture. *Adv. Mater.* **2014**, *26*, 3644−3648.
(39) Evans, J. D.; Huang, D. M.; Hill, M. R.; Sumby, C. J.; Thornton, A. W.; Doonan, C. J. Feasibility of Mixed Matrix Membrane Gas Separations Employing Porous Organic Cages. *J. Phys. Chem. C* **2014**, *118*, 1523−1529.

DOI: 10.1021/acsami.5b04148
ACS Appl. Mater. Interfaces 2015, 7, 15561−15569

(40) Rangel, E. R.; Maya, E. M.; Sánchez, F.; Abajo, J. D.; Campa, J. G. D. L. Gas Separation Properties of Mixed-Matrix Membranes Containing Porous Polyimides Fillers. *J. Membr. Sci.* **2013**, *447*, 403−412.
(41) Qian, H. D.; Zheng, J. F.; Zhang, S. B. Preparation of Microporous Polyamide Networks for Carbon Dioxide Capture and Nanofiltration. *Polymer* **2013**, *54*, 557−564.
(42) Yong, W. F.; Li, F. Y.; Xiao, Y. C.; Chung, T. S.; Tong, Y. W. High Performance PIM-1/Matrimid Hollow Fiber Membranes for CO_2/CH_4, O_2/N_2 and CO_2/N_2 Separation. *J. Membr. Sci.* **2013**, *443*, 156−169.
(43) Bushell, A. F.; Attfield, M. P.; Mason, C. R.; Budd, P. M.; Yampolskii, Y.; Starannikova, L.; Rebrov, A.; Bazzarelli, F.; Bernardo, P.; Jansen, J. C.; Lanč, M.; Friess, K.; Shantarovich, V.; Gustov, V.; Isaeva, V. Gas Permeation Parameters of Mixed Matrix Membranes Based on The Polymer of Intrinsic Microporosity PIM-1 and The Zeolitic Imidazolate Framework ZIF-8. *J. Membr. Sci.* **2013**, *427*, 48−62.
(44) Coker, D. T.; Freeman, B. D. Modeling Multicomponent Gas Separation Using Hollow-Fiber Membrane Contactors. *AIChE J.* **1998**, *44*, 1289−1302.
(45) Gabelman, A.; Hwang, S. T. Hollow Fiber Membrane Contactors. *J. Membr. Sci.* **1999**, *159*, 61−106.
(46) Mahajan, R.; Koros, W. J.; Thundyil, M. Mixed Matrix Membranes: Important and Challenging! *Membr. Technol.* **1999**, *105*, 6−8.
(47) Blades, H. Dry Jet Wet Spinning Process. U.S. Patent 3,767,756, 1973.
(48) Husain, S. Mixed Matrix Dual Layer Hollow Fiber Membranes for Natural Gas Separation. Ph.D. Dissertation, Georgia Institute of Technology, Atlanta, 2006.
(49) Sonogashira, K.; Tohda, Y.; Hagihara, N. A Convenient Synthesis of Acetylenes: Catalytic Substitutions of Acetylenic Hydrogen with Bromoalkenes, Iodoarenes and Bromopyridines. *Tetrahedron Lett.* **1975**, *16*, 4467−4470.
(50) Yang, Q.; Zhong, C. Molecular Simulation of Carbon Dioxide/Methane/Hydrogen Mixture Adsorption in Metal-Organic Frameworks. *J. Phys. Chem. B* **2006**, *110*, 17776−17783.
(51) Mosher, K.; Liu, Y.; Wilcox, J. *The Impact of Pore Size on Methane and CO_2 Adsorption in Carbon*; Stanford University Press: Stanford, CA, 2011.
(52) Du, N. Y.; Park, H. B.; Robertson, G. P.; Dal-Cin, M. M.; Visser, T.; Scoles, L.; Guiver, M. D. Polymer Nanosieve Membranes for CO_2-Capture Applications. *Nat. Mater.* **2011**, *10*, 372−375.
(53) Merkel, T. C.; Bondar, V. I.; Nagai, K.; Freeman, B. D.; Pinnau, I. Gas Sorption, Diffusion, and Permeation in Poly(dimethylsiloxane). *J. Polym. Sci., Part B: Polym. Phys.* **2000**, *38*, 415−434.
(54) Spycher, N. F.; Reed, M. H. Fugacity Coefficients of H_2, CO_2, CH_4, H_2O and of H_2O-CO_2-CH_4 Mixtures: A Virial Equation Treatment for Moderate Pressures and Temperatures Applicable to Calculations of Hydrothermal Boiling. *Geochim. Cosmochim. Acta* **1988**, *52*, 739−749.

DOI: 10.1021/acsami.5b04148
ACS Appl. Mater. Interfaces 2015, 7, 15561−15569